

Entanglement spectroscopy of SU(2)-broken phases in two dimensions

F. Kolley,¹ S. Depenbrock,¹ I. P. McCulloch,² U. Schollwöck,¹ and V. Alba¹

¹*Department of Physics and Arnold Sommerfeld Center for Theoretical Physics, Ludwig-Maximilians-Universität München, D-80333 München, Germany*

²*School of Physical Sciences, The University of Queensland, Brisbane, QLD 4072, Australia*

(Received 11 August 2013; published 30 October 2013)

In magnetically ordered systems, the breaking of SU(2) symmetry in the thermodynamic limit is associated with the appearance of a special type of low-lying excitations in finite-size energy spectra, the so-called tower of states (TOS). In the present work, we numerically demonstrate that there is a correspondence between the SU(2) tower of states and the lower part of the *ground-state* entanglement spectrum (ES). Using state-of-the-art density matrix renormalization group (DMRG) calculations, we examine the ES of the 2D antiferromagnetic J_1 - J_2 Heisenberg model on both the triangular and kagome lattice. At large ferromagnetic J_2 , the model exhibits a magnetically ordered ground state. Correspondingly, its ES contains a family of low-lying levels that are reminiscent of the energy tower of states. Their behavior (level counting, finite-size scaling in the thermodynamic limit) sharply reflects TOS features, and is characterized in terms of an effective entanglement Hamiltonian that we provide. At large system sizes, TOS levels are divided from the rest by an entanglement gap. Our analysis suggests that (TOS) entanglement spectroscopy provides an alternative tool for detecting and characterizing SU(2)-broken phases using DMRG.

DOI: [10.1103/PhysRevB.88.144426](https://doi.org/10.1103/PhysRevB.88.144426)

PACS number(s): 05.30.-d, 03.67.-a, 75.40.Mg

I. INTRODUCTION

Recent years have witnessed an increasing interest in entanglement related quantities (and quantum information concepts in general) as new tools to understand the behavior of quantum many-body systems.¹ Very recently, the entanglement spectrum² (ES) has established itself as a new prominent research topic. Considering the bipartition of a system into parts A and B , the ES, $\{\xi_i\}$, is constructed from the Schmidt decomposition

$$|\psi\rangle = \sum_i e^{-\xi_i/2} |\psi_i^A\rangle \otimes |\psi_i^B\rangle. \quad (1)$$

Here, $|\psi\rangle$ is the ground state, and the states $|\psi_i^A\rangle$ ($|\psi_i^B\rangle$) provide an orthonormal basis for subsystem A (B). The ES $\{\xi_i\}$ can also be interpreted as the spectrum of the so-called entanglement Hamiltonian $\mathcal{H}_E \equiv -\ln \rho_A$, where the reduced density matrix ρ_A is obtained by tracing out part B in the full system density matrix $|\psi\rangle\langle\psi|$.

While in one-dimensional (1D) systems the structure of ES is related to integrability³⁻⁵ and (for gapless systems) to conformal invariance,⁵⁻⁸ higher dimensions are by far less explored. In particular, most of the recent literature on two-dimensional (2D) systems focused on ES properties in topological phases.^{2,9}

In more standard (i.e., nontopological) 2D systems, although some results are available¹⁰⁻¹³, much less is known. Nevertheless, it has been established recently that in systems displaying ordered ground states (in the thermodynamic limit), with breaking of a *continuous* symmetry, the lower part of the ES is in correspondence with the so-called “tower of states” (TOS) spectrum.^{14,15} This describes the low-energy structure of *finite-size* spectra in systems that spontaneously break a continuous symmetry. In combination with exact

diagonalization techniques, tower of states spectroscopy is routinely used to detect symmetry broken phases.¹⁶⁻²³

So far, tower of states structures in ES have only been observed numerically in the superfluid phase of the 2D Bose-Hubbard model,¹⁵ where the formation of a Bose condensate is associated with the breaking of a U(1) gauge symmetry (reflecting conservation of the total number of particles in finite systems). The resulting TOS spectrum, however, (and the lower part of the ES thereof) is “trivial” with one level (excitation) per particle number sector.¹⁵

Richer behavior is expected in SU(2)-broken phases, where different SU(2) breaking patterns (i.e., Néel states) give rise to different structures in the energy TOS. For instance, for Néel order with more than two ferromagnetic sublattices [associated with full breaking of SU(2)], the spin-resolved TOS spectrum exhibits a family of levels (i.e., more than one level) in each spin sector.²⁴

In this paper, we demonstrate that this richer structure is reflected in the lower part of the ES, providing a more stringent check of the correspondence between tower of states and entanglement spectrum. To be specific, we focus on the 2D Heisenberg model with nearest and next-nearest-neighbor interaction (J_1 and J_2 , respectively). We consider both the kagome (KHA) and the triangular lattice (THA), restricting ourselves to ferromagnetic J_2 ($J_2 = -1$), to ensure a magnetically ordered ground state on both lattices. In order to take advantage of the SU(2) invariance of the model, we employ non-Abelian [SU(2)-symmetric] density matrix renormalization group (DMRG) simulations.

Our results are summarized as follows. In both the J_1 - J_2 KHA and THA, in the symmetry broken phase, the lower part of the ES (resolved with respect to the block spin S_A) sharply reflects the same TOS structure as the physical bulk Hamiltonian. Low-lying ES levels are organized into families, each corresponding to a different S_A and containing more than

one level (in contrast to the Bose-Hubbard model where the TOS structure is “trivial”). The counting of TOS levels in each S_A sector reflects the corresponding counting in the energy TOS.

The TOS-like structure is divided from higher levels by an entanglement gap, which remains finite (or vanishes logarithmically) in the thermodynamic limit (as found in the Bose-Hubbard ES¹⁵). All ES levels below the gap are degenerate in the thermodynamic limit, and their finite-size behavior is fully understood within the framework of the TOS-ES correspondence. Oppositely, for finite systems, ES levels within each TOS family are not exactly degenerate (similarly to energy TOS²⁴) giving rise to intriguing entanglement (TOS) substructures. The main features of TOS levels (TOS substructures, finite-size behaviors) are quantitatively characterized by an approximate mapping between the entanglement Hamiltonian and the physical bulk Hamiltonian.

Finally, as an additional point, we investigate the effect of boundary conditions on the TOS structure. To this purpose, we consider the ES of the J_1 - J_2 KHA ($J_2/J_1 = -1$) on the torus geometry, which has the net effect of introducing two boundaries (edges) between subsystem A and B . We find that in $SU(2)$ broken phases, the structure of the ES is weakly affected by boundaries, reflecting the bulk origin of TOS excitations. This is dramatically different in gapped phases^{4,15} or in FQH systems⁹ where the ES obtained from bipartitions with multiple edges can be constructed combining single-edge ES.

On the methodological side, our analysis suggests that entanglement TOS spectroscopy, combined with $SU(2)$ symmetric DMRG, could provide a potentially powerful tool to detect and characterize magnetically ordered ground states. Also, while conventional energy TOS spectroscopy requires the calculation of several excited states (which is computationally expensive in DMRG), ES are readily obtained from *ground-state* wave functions only.

The paper is organized as follows. Section II introduces the J_1 - J_2 Heisenberg model on both the kagome and triangular lattice. Some basic facts about conventional (energy) tower of states spectroscopy in $SU(2)$ broken phases are given in Sec. III. In Sec. IV, we establish the correspondence between the tower of states and the low-lying part of the ES (cf. Sec. IV A). This is numerically verified in Sec. IV B for the J_1 - J_2 kagome and triangular lattice Heisenberg models. The fine structure (i.e., entanglement substructures) of ES levels building the TOS is detailed in Sec. IV C. Finite-size behavior of the (TOS) ES and its dependence on boundary conditions are discussed in Sec. V. Section VI concludes the paper.

II. MODELS AND METHOD

In this paper, we consider the two-dimensional spin- $\frac{1}{2}$ Heisenberg model with both nearest and next-nearest-neighbor interactions (J_1 - J_2), defined by the $SU(2)$ symmetric Hamiltonian

$$\mathcal{H} = J_1 \sum_{\langle i,j \rangle} \mathbf{S}_i \cdot \mathbf{S}_j + J_2 \sum_{\langle\langle i,k \rangle\rangle} \mathbf{S}_i \cdot \mathbf{S}_k. \quad (2)$$

Here, \mathbf{S}_i are spin- $\frac{1}{2}$ operators and $\langle i,j \rangle$, $\langle\langle i,k \rangle\rangle$ denote, respectively, nearest-neighbor and next-nearest-neighbor sites

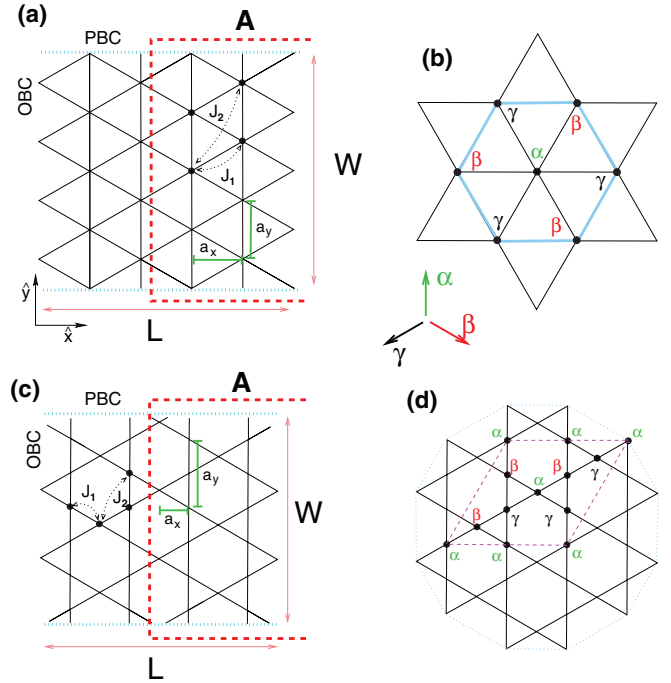


FIG. 1. (Color online) The J_1 - J_2 Heisenberg model on the triangular (THA) and kagome (KHA) lattices. (a) Example of triangular cylinder of length L and width W (measured respectively in units of a_x and a_y). Total number of sites is given as $W \times L$. Spins are at the vertices of the lattice. Periodic boundary conditions are used along the vertical direction. J_1 (J_2) is the interaction strength between nearest (next-nearest) neighbor spins. In this work we restrict ourselves to antiferromagnetic (ferromagnetic) J_1 (J_2) (i.e., $J_1 > 0$, $J_2 < 0$). The dashed line is to illustrate the bipartition into two subsystems. (b) Ordering pattern of the THA. Three possible orientations of the sublattice spins are denoted as α, β, γ . The angle formed by any pair of spins is $2\pi/3$. (c) Heisenberg J_1 - J_2 on the kagome lattice (KHA). Total number of spins is now $3 \times W \times L$. (d) Ordering pattern of the J_1 - J_2 KHA ($\sqrt{3} \times \sqrt{3}$ structure). Dashed line is to highlight the nine spins unit cell.

on the lattice. We consider both triangular and kagome cylinders of size $W \times L$ [see Figs. 1(a) and 1(c), respectively] with periodic boundary conditions along the vertical direction. We choose $J_1 > 0$ (antiferromagnetic nearest-neighbor interactions) and $J_2 < 0$ (ferromagnetic next-nearest-neighbor interaction). Clearly, a large negative J_2 favors the formation of ferromagnetic sublattices [cfs. Figs. 1(a) and 1(c)] and magnetic order.²⁴ Here, in particular, we restrict ourselves to $J_2/J_1 = -1$ to ensure a magnetically ordered ground state on both the triangular and kagome lattice.

a. The triangular lattice. The ground state of the J_1 - J_2 Heisenberg model on the triangular lattice (THA) exhibits at $J_2/J_1 = -1$ (at a semiclassical level, i.e., considering large spins $S \gg 1/2$) the so-called 120° structure. This is depicted in Fig. 1(b) and consists of three ferromagnetic sublattices (associated with full breaking of spin rotational invariance). Spins on the same sublattice are parallel, while the angle between spins in different sublattices is 120° . A possible choice of ordering pattern is shown in Fig. 1 (spin orientations are denoted as α, β, γ). For spins $S = 1/2$ (which is the case of interest here) quantum fluctuations are not strong

enough to destroy the magnetic order and the 120° structure survives. One should mention that this remains true at arbitrary $J_2 \leq 0$, as confirmed by spin-wave calculations,^{25–30} Green's function Monte Carlo,³¹ series expansions,³² tower of states spectroscopy,¹⁶ and recent DMRG calculations.³³

b. The kagome lattice. Much less is known about the phase diagram of the J_1 - J_2 Heisenberg model on the kagome lattice (KHA) [cf. Fig. 1(c)]. At large ferromagnetic $J_2 < 0$ (in particular at $J_2/J_1 = -1$) the ground state exhibits magnetic order *à la Néel* with spontaneous breaking of SU(2) symmetry. The selected ordering pattern is the $\sqrt{3} \times \sqrt{3}$ state [cf. Fig. 1(d)]. As for the THA [Fig. 1(b)], three ferromagnetic sublattices are present, although the unit cell (highlighted with the dashed line in the figure) is now larger (it contains nine spins).

One should mention that, while it is well established that the $\sqrt{3} \times \sqrt{3}$ order survives at smaller J_2 (i.e., at $J_2 > -1$),¹⁹ it is still a challenging task to determine the phase diagram of the J_1 - J_2 KHA in the limit $J_2 \approx 0$. In particular, the nature of the ground state of the pure kagome Heisenberg antiferromagnet (i.e., at $J_2 = 0, J_1 > 0$) is still debated. Several valence bond crystals^{34–40} and spin liquid ground states^{41–53} (both gapless and gapped) have been proposed. Remarkably, recent state-of-the-art DMRG calculations have provided robust evidence of a gapped Z_2 topological spin liquid.^{54,55} Interestingly, there is also evidence that the spin liquid behavior might survive at small positive J_2 with the formation of an extended spin liquid region.⁵⁶

c. Entanglement spectrum (ES). In order to calculate the ES we consider the bipartition of the system (cylinders in Fig. 1) into two equal parts A and B , using a vertical cut [dashed line along the y direction in Figs. 1(a) and 1(c)]. As a consequence, the boundary between A and B is a circumference of length W . The total subsystem spin S_A^z is a good “quantum number” for the ES and can be used to label ES levels, i.e., ES levels are organized into SU(2) multiplets. Equivalently, the entanglement Hamiltonian \mathcal{H}_E (or the reduced density matrix ρ_A) exhibits a block structure, each block corresponding to a different S_A sector.

d. Ground-state search (DMRG method). The ground state is obtained in a matrix product state form by using state-of-the-art SU(2)-symmetric single-site DMRG.^{57–59} DMRG is a variational method in the ansatz space spanned by matrix product states (MPS). The method allows one to find the ground state of one-dimensional (1D) systems efficiently even for large system sizes. It has also been successfully applied to two-dimensional (2D) lattices by mapping the short-ranged 2D Hamiltonian exactly to a long-ranged 1D one.^{33,54,55,60–63} Here, to ensure independence on the actual mapping, we performed several calculations using different mappings. DMRG computational cost scales roughly exponentially with the entanglement entropy and favors open (OBC) over periodic boundary conditions (PBC). The conventional compromise, taken also by us, is to consider cylinders, i.e., PBC along the short direction (circumference W) and OBC along the long direction (length L) where boundary effects are less important. Computational cost is then dominated exponentially by W . Exploiting the power of the non-Abelian formulation we were able to simulate the systems using up to 5000 ansatz states, corresponding to roughly 20 000 states in an Abelian U(1)

DMRG, allowing us to obtain the ground state of (2) with high accuracy, even for cylinders with $W = 9$ (for the J_1 - J_2 THA) or fully periodic tori. One should also mention that in SU(2)-broken phases the large entanglement gap, which divides the TOS ES levels from the rest, reduces significantly the effective number of states needed to get well converged ground states.

III. TOWER OF STATES SPECTROSCOPY IN SU(2) BROKEN PHASES

Due to its manifest spin rotational invariance, the finite-size spectrum of (2) can be decomposed into the irreducible representations of SU(2), using the eigenvalue S of the total spin S^2 to label energy levels (and eigenstates). The resulting spin-resolved spectrum shows striking signatures of the SU(2) breaking (happening in the thermodynamic limit). Exact diagonalization studies¹⁹ demonstrated that at $J_2/J_1 = -1$ in each spin sector S there is a family of (low-lying) levels, which are clearly separated from the rest by an energy gap (at least for large systems). These are called “quasidegenerate joint states” (QDJS) in Ref. 17 and form the TOS structure.

The number N_S of TOS levels in each spin sector is related to the Néel state selected in the thermodynamic limit. For instance, Néel ordering with two ferromagnetic sublattices (as for the Heisenberg antiferromagnet on the square lattice²⁴), corresponding to the breaking of SU(2) down to U(1), implies $N_S = 2S + 1$. On the other hand, a complete breaking of SU(2) (for instance, Néel ordering with more than two ferromagnetic sublattices, as for both the THA and KHA, cf. Fig. 1) implies $N_S > 2S + 1$ ²⁴ (see also below).

The TOS structure can be obtained as the lowest energy manifold of an effective Hamiltonian \mathcal{H}_T (“quantum top”), which, for Néel order with three ferromagnetic sublattices a, b, c , reads^{16,64–67}

$$\begin{aligned} \mathcal{H}_T &= \frac{1}{2\chi V} (\mathbf{S}^2 - \mathbf{S}_a^2 - \mathbf{S}_b^2 - \mathbf{S}_c^2) \\ &\equiv \frac{1}{\chi V} (\mathbf{S}_a \cdot \mathbf{S}_b + \mathbf{S}_a \cdot \mathbf{S}_c + \mathbf{S}_b \cdot \mathbf{S}_c). \end{aligned} \quad (3)$$

Here, χ is the spin susceptibility, V the volume (i.e., total number of sites), and $\mathbf{S} (\mathbf{S}_{a,b,c})$ the total spin of the system (sublattice). Notice that one could think of (3) as an effective Heisenberg coupling between $\mathbf{S}_a, \mathbf{S}_b, \mathbf{S}_c$, acting as collective degrees of freedom. As the lowest energy manifold of (3) is obtained choosing $S_a = S_b = S_c = V/3 \times 1/2$, one readily obtains the number of TOS levels per spin sector as $N_S = (2S + 1)^2$.¹⁷ These, according to (3), are degenerate with energy given as

$$E_T(S) = \frac{1}{2\chi V} S(S + 1), \quad (4)$$

where we neglected the sublattice contributions, keeping only S dependent terms. Plotted as function of $S(S + 1)$, TOS levels show the typical “Pisa tower” (linear) structure,¹⁷ with a vanishing (as $1/V$) “slope.”

Still, one should think of (3) only as the low-energy approximation of (2). To go beyond one can split \mathcal{H} as $\mathcal{H} = \mathcal{H}_T + \mathcal{H}'$ with \mathcal{H}' a (higher-energy) correction to \mathcal{H}_T . Specifically, one has $\mathcal{H}' \approx \mathcal{H}_{\text{sw}}, \mathcal{H}_{\text{sw}}$ describing levels immediately above the

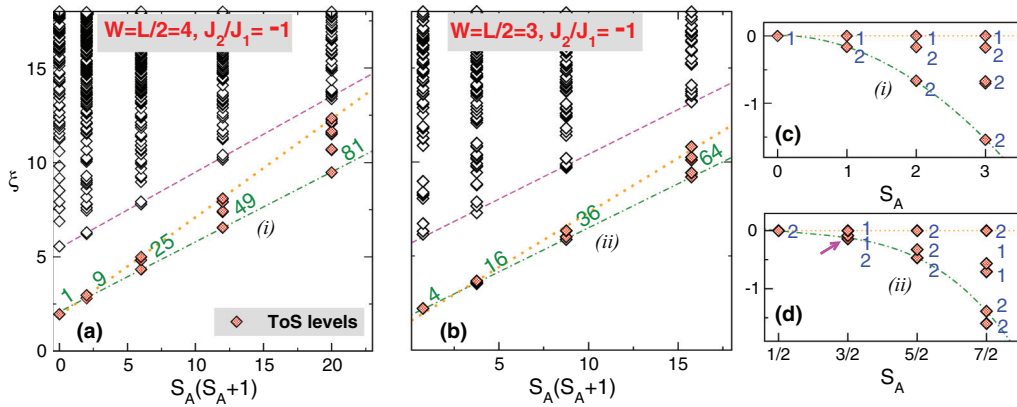


FIG. 2. (Color online) Tower of states (TOS) structure in the ES of the J_1 - J_2 kagome Heisenberg model (KHA) at $J_2/J_1 = -1$. Half-system ES levels ξ vs $S_A(S_A + 1)$, with S_A the block spin. Symbols are DMRG data for the KHA on a cylinder with $W = L/2 = 4$ (a) and $W = L/2 = 3$ (b), same scale used on the y axis. Each point corresponds to a degenerate SU(2) multiplet ($2S_A + 1$ levels). Filled symbols denote levels building the TOS. Dashed-dotted line is to highlight the behavior as $S_A(S_A + 1)$. TOS levels are divided from the rest (levels above the dashed line in the figure) by an entanglement gap. Accompanying numbers are the numbers of TOS ES levels. (c) and (d) Enlarged view of the TOS structures (i) and (ii) shown, respectively, in (a) and (b). In each S_A sector, ES levels are shifted by the value of the highest level [dotted line in (a) and (b)]. ES levels are plotted against the block spin S_A . The number of degenerate SU(2) multiplets is reported in blue. In (d), the arrow is to stress the presence of isolated (i.e., unpaired) multiplets (see also multiplets at $S_A = 7/2$).

TOS structure. These correspond to spin waves (Goldstone modes) and possess a linear dispersion, implying (using that momentum is discretized on a finite lattice as $1/\sqrt{V}$) $\mathcal{H}_{sw} \approx 1/\sqrt{V}$. As a striking consequence, the TOS spectrum (4) is divided from higher energy levels by an apparent gap at $V \rightarrow \infty$.

Moreover, since in general $[\mathcal{H}_T, \mathcal{H}'] \neq 0$, the degeneracy within each TOS manifold at spin S [cf. (4)] is partly lifted, implying that \mathcal{H}_T [cf. (3)] has to be modified. Notice that, in principle, the final degeneracy structure can be predicted using group symmetry analysis.¹⁷ Remarkably, in the limit of large systems, \mathcal{H}_T can be mapped to the anisotropic “quantum top”:¹⁷

$$\mathcal{H}_T = \frac{\mathbf{S}^2}{2V\chi_\perp} + \frac{(S^{z'})^2}{2V} \left(\frac{1}{\chi_\parallel} - \frac{1}{\chi_\perp} \right). \quad (5)$$

Here, $S^{z'} \in [-S, S]$ is the component of the total spin along the third axis z' of the “quantum top” (not necessarily the z axis in the laboratory frame), while χ_\parallel and χ_\perp denote, respectively, the parallel and transverse susceptibilities, which measure the response to magnetic fields in the plane of the spins and in the perpendicular one. Notice that both terms in (5) are $\sim 1/V$. One has for large system sizes $\chi_\perp \neq \chi_\parallel$, reflecting the tendency towards magnetic order and the system response becoming anisotropic. The degeneracy structure of TOS multiplets is now readily obtained from (5); in the sector with half-integer S there are $S + 1/2$ pairs of degenerate multiplets, whereas for integer S one has S degenerate pairs and an extra isolated multiplet [corresponding to $S^{z'} = 0$ in (5)].

IV. ENTANGLEMENT SPECTRA IN SU(2)-BROKEN PHASES

In this section, we numerically demonstrate that in SU(2)-broken phases the information contained in the energy tower of states is nicely embodied in the lower part of the

ground-state entanglement spectrum (TOS-ES correspondence). This section is organized as follows. In Sec. IV A, we establish the TOS-ES correspondence,^{14,15} which is expressed as a mapping between the TOS Hamiltonian \mathcal{H}_T and the entanglement Hamiltonian \mathcal{H}_E . This is supported numerically in Sec. IV B highlighting TOS structures in the ES of the J_1 - J_2 KHA and THA (at $J_2/J_1 = -1$). Our main results are illustrated in Figs. 2 and 3. Finally, the fine structure (TOS substructure) of the TOS-related levels is detailed in Sec. IV C.

A. TOS-ES correspondence

It has been suggested recently that in systems breaking a *continuous* symmetry in the thermodynamic limit the lower part of the (ground-state) ES has the same structure as the TOS energy spectrum.¹⁴ Here, we restrict ourselves to the situation of SU(2) symmetry breaking. The correspondence can be expressed as a mapping between an effective entanglement Hamiltonian \mathcal{H}_E (describing the lower part of the ES) and the TOS Hamiltonian \mathcal{H}_T . Specifically, one has¹⁴

$$\mathcal{H}_E \propto \mathcal{H}_T(A)/T_E, \quad (6)$$

where \mathcal{H}_T is restricted to the degrees of freedom of subsystem A and $T_E \approx v_s/\sqrt{V}$ is an effective “entanglement temperature,” which reflects the presence of gapless excitations (spin waves) arising from the breaking of the SU(2) symmetry (here v_s is the spin wave velocity). The behavior $T_E \approx 1/\sqrt{V}$ originates from the linear dispersion of spin waves and the momentum quantization as $1/\sqrt{V}$ on a finite lattice.

From (6) two remarkable properties can be derived. First, using that $\mathcal{H}_T \sim 1/V$ [cf. (5)] and $T_E \sim 1/\sqrt{V}$, one obtains that the spacing between the ES levels building the TOS structure is vanishing as $1/\sqrt{V}$ in the thermodynamic limit. Additionally, including the spin-wave contributions in the energy spectrum, i.e., replacing $\mathcal{H}_T \rightarrow \mathcal{H}_T + \mathcal{H}_{sw}$, and assuming that ES levels above the TOS structure are

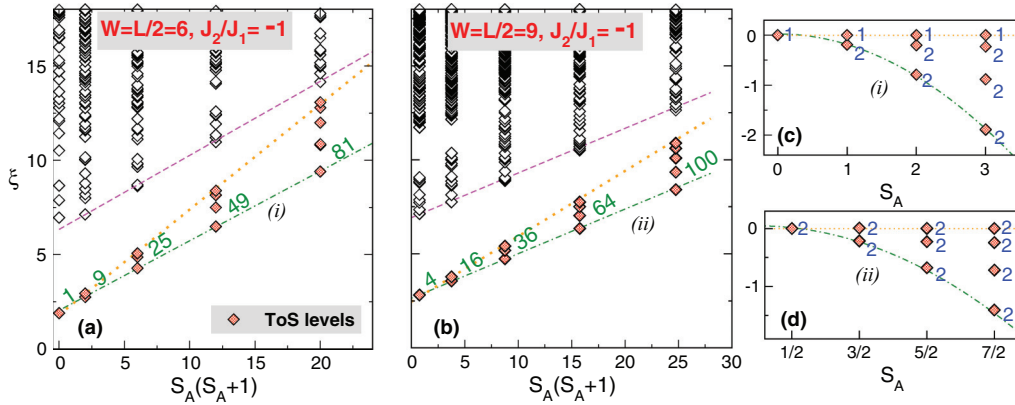


FIG. 3. (Color online) Tower of states (TOS) structure in the ES of the J_1 - J_2 Heisenberg model on the triangular lattice (THA) ($J_2/J_1 = -1$). ES for half of the system: ES levels ξ vs $S_A(S_A + 1)$, S_A being the total subsystem spin. Symbols are DMRG data for cylinders with $W = L/2 = 6$ (a) and $W = L/2 = 9$ (b) (cf. Fig. 1). Each point corresponds to a degenerate SU(2) multiplet ($2S_A + 1$ levels). Filled symbols denote the ES levels forming the TOS. Dashed-dotted line highlights the TOS behavior as $S_A(S_A + 1)$. TOS levels are divided from the rest of the spectrum (levels above the dashed line) by an entanglement gap. The total number of ES levels in each S_A sector is reported in green (numbers accompanying ES multiplets). (Right) Enlarged view of the TOS structures in (a) and (b), ES plotted vs S_A . ES levels at each S_A are shifted by the highest level [dotted lines in (a) and (b)]. Lines are guides to the eye as in (a) and (b). Accompanying numbers denote the number of degenerate multiplets.

spin-wave-like, from (6) one obtains \mathcal{H}_E as

$$\mathcal{H}_E \sim (\mathcal{H}_T + \mathcal{H}_{sw})/T_E. \quad (7)$$

The behaviors $T_E \sim 1/\sqrt{V}$ and $\mathcal{H}_{sw} \sim 1/\sqrt{V}$ now suggest the formation of a finite gap (in the limit $V \rightarrow \infty$) between the TOS structure and the higher part of the ES. However, one should stress that a logarithmic vanishing of the entanglement gap, also suggested by field theoretical calculations,⁶⁸ cannot be excluded. These findings (presence of a finite gap in the ES and the finite-size behavior of the TOS structure) have been confirmed in Ref. 15 for the 2D Bose-Hubbard model in the superfluid phase.

Finally, it is interesting to discuss how TOS structures affect the behavior of the entanglement entropy. The fact that the low-energy part of (2) (and its ground state) can be described by an effective free bosonic theory (\mathcal{H}_{sw} , cf. Sec. III) suggests that an area law behavior should be expected (cf. 1 and references therein for a discussion of area laws in free systems). On the other hand, the breaking of a continuous symmetry gives rise to additive logarithmic corrections to the entropy,¹⁴ which, for instance, have been observed numerically in the 2D Heisenberg antiferromagnet on the square lattice.⁶⁹⁻⁷¹ At the level of the ES, these corrections are associated with the TOS structure, while the area law arises from ES levels above the entanglement gap. Note that the entanglement gap is typically large deep in a SU(2)-broken phase (see Sec. IV B), implying that the TOS levels give the dominant contribution to the entanglement entropy, while the area law behavior is recovered only asymptotically for large system sizes.

B. DMRG results

a. J_1 - J_2 kagome Heisenberg (KHA). We start discussing the tower of states structures in the ES of the KHA at $J_2/J_1 = -1$. Figure 2 plots the ES (DMRG data) obtained from the ground state of the KHA on cylinders [cf. Fig. 1(c)] with fixed

aspect ratio $W/L = 1/2$ and $W = 3, 4$ (respectively, center and left panels in Fig. 2). Total number of spins in the subsystem is given as $3W^2$ (ES is for half cylinder) and is even (odd) for $W = 4(3)$. ES levels ξ are plotted versus $S_A(S_A + 1)$, S_A being the total spin of subsystem A .

In each spin sector S_A , a family of low-lying ES multiplets [each point corresponds to an SU(2) multiplet of degenerate levels, filled rhombi in Fig. 2] is well separated from higher levels by a gap. The total number of levels below the gap (TOS levels) in each sector S_A is given as $(2S_A + 1)^2$ (numbers accompanying ES multiplets in the figure), clearly reflecting the corresponding multiplicity [as $(2S + 1)^2$] in the energy tower of states (cf. Sec. III). Also, the lower part of the TOS levels exhibits the typical TOS behavior as $S_A(S_A + 1)$ (see dashed-dotted lines in Fig. 2) in agreement with (4) and (6). The entanglement gap appears to be constant as a function of S_A (dashed line denotes levels immediately above the TOS structure), similarly to what is observed in energy TOS structures²⁴ and in the ES of the 2D Bose-Hubbard.¹⁵

Interestingly, at each fixed S_A , the TOS levels are not exactly degenerate, and further substructures appear, reflecting the presence of the second term in (5). TOS substructures are better highlighted in Figs. 2(c) and 2(d) showing an enlarged view of the TOS levels [same DMRG data as in panels (a) and (b)]. In each sector S_A we shifted the ES by subtracting the value of the largest level [dashed-dotted and dashed lines are guides to the eye as in panels (a) and (b)]. Reported numbers correspond now to the number of degenerate SU(2) multiplets.

According to (6), the degeneracy structure in the TOS part of the ES is the same as that in the energy tower of states. At large system sizes and *integer* S_A (i.e., even number of spins in A) the TOS ES levels are organized in pairs of degenerate multiplets, apart from one isolated multiplet at the top of each S_A sector. This is clearly supported in Fig. 2(c).

On the other hand, for *half-integer* S_A only pairs of degenerate multiplets are expected [cf. (5)]. Figure 2(d) shows the

TOS ES levels for the kagome cylinder with $W = 3$ (i.e., 27 spins in subsystem A). Although a clear tendency towards the formation of pairs is visible (levels at the top of the structure form pairs, while in panel (c) one has one isolated multiplet), some deviations are observed. For instance [see arrow in Fig. 2(d)], one has in the sector with $S_A = 3/2$ four SU(2) multiplets, but only two form a pair. Similarly, in the sector with $S_A = 7/2$ two isolated multiplets are visible. Since (5) is valid only in the asymptotic (i.e., large V) regime, these deviations have to be understood as finite-size effects. Indeed, we checked that at $W = 5$ (i.e., 75 spins in subsystem A) all the (TOS) multiplets form degenerate pairs (at least in the first few S_A sectors).

b. J_1 - J_2 triangular Heisenberg (THA). Further evidence supporting the TOS-ES scenario is provided in Fig. 3 considering the 2D J_1 - J_2 Heisenberg model on the triangular lattice (THA). The ground-state ordering pattern [120° structure, cf. Fig. 1(b)] contains three ferromagnetic sublattices [full breaking of SU(2)] and the same tower of states structure as for the kagome is expected.

Figure 3 plots DMRG data for the ES of the THA on the cylinder [at fixed aspect ratio $W/L = 1/2$ with $W = 6$ and $W = 9$, respectively, in panel (a) and (b)]. ES is for half of the cylinder. Notice that we could access larger system sizes than for the kagome (compare with Fig. 2). This allows us to resolve the TOS multiplets (corresponding to 100 ES levels) at $S_A = 9/2$. As for the kagome ES (cf. Fig. 2), the lower part of the ES (filled symbols in the figure) is divided from the rest of the spectrum by an entanglement gap and exhibits the typical TOS behavior as $S_A(S_A + 1)$.

The correct SU(2) TOS level counting (i.e., number of TOS levels in each spin sector S_A) as $(2S_A + 1)^2$ is fully reproduced. The fine structure of TOS multiplets (TOS substructure) is highlighted in Figs. 3(c) and 3(d). Remarkably, for odd number of spins in A all TOS levels are organized into pairs of degenerate multiplets [cf. Fig. 3(d)], whereas for even ones, there is an isolated ES multiplet at the top of the structure [cf. Fig. 3(c)], signaling that finite size corrections are somehow smaller than in the kagome ES (cf. Fig. 2).

C. Tower of states entanglement substructures

We now analyze quantitatively the structure of the TOS ES multiplets. We start with observing that in the limit of large cylinders the effective entanglement Hamiltonian \mathcal{H}_E describing the TOS structure is obtained from (5) and (6) as

$$\mathcal{H}_E \sim \frac{S_A^2}{v_s \chi_\perp W} - \frac{(S_A^z)^2}{v_s W} \left(\frac{1}{\chi_\perp} - \frac{1}{\chi_\parallel} \right), \quad (8)$$

where we used that $\sqrt{V} \approx W$. While the first term in (8) gives the TOS behavior as $S_A(S_A + 1)$ (cf. Figs. 2 and 3), with $(2S_A + 1)^2$ degenerate levels at each S_A , the second gives rise to the substructures in Figs. 2, 3(c), and 3(d).

These are shown in Fig. 4 plotting the shifted ES levels (same DMRG data as in Figs. 2, 3(c), and 3(d)) for both the triangular and kagome J_1 - J_2 Heisenberg model at $J_2/J_1 = -1$. Since ES levels in each sector S_A are shifted by the value of the largest level, the contribution of the first term $[\sim S_A(S_A + 1)]$ in (8) has to be neglected. Thus, structures

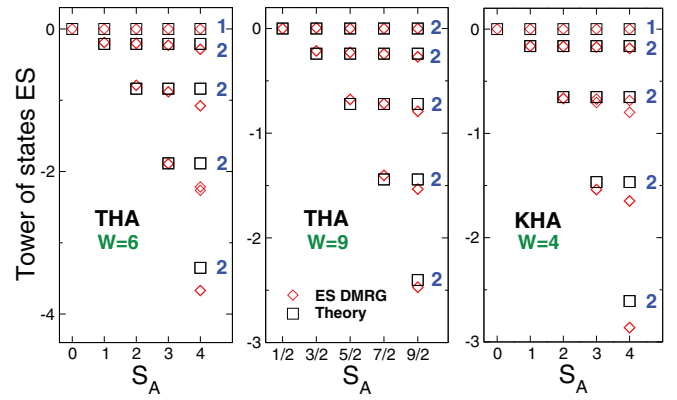


FIG. 4. (Color online) TOS entanglement substructures. ES of the Heisenberg J_1 - J_2 model on the triangular (THA) and kagome (KHA) lattice: ES levels ξ vs the total spin S_A of subsystem A . Each point corresponds to a degenerate SU(2) multiplet ($2S_A + 1$ levels). Only multiplets building the TOS structure are shown. In each spin sector with fixed S_A , ES multiplets are shifted by the value of the largest level. Rhombi are the same DMRG data as in Figs. 2, 3(c), and 3(d). The squares denote the (one parameter) fit to the theoretical prediction [cf. (8)] in the limit of large systems ($W, L \rightarrow \infty$). In all panels, accompanying numbers denote the number of degenerate SU(2) multiplets.

appearing in Fig. 4 are described by $\alpha[(S_A^z)^2 + s_0]$, being $\alpha \sim (\chi_\parallel - \chi_\perp)/(v_s W \chi_\perp \chi_\parallel)$, and $s_0 = 0(-1/4)$ for integer(half-integer) values of S_A .

This scenario is confirmed fitting TOS levels in Fig. 4 to $\alpha[(S_A^z)^2 + s_0]$, with α the only fitting parameter. For the THA (including in the fit only the ES towers with $S_A \leq 3$), it is $\alpha \approx 0.21$, while for $W = 9$ (now including all the ES levels with $S_A \leq 9/2$) one obtains $\alpha \approx 0.12$. Notice that it is $0.12/0.21 \sim 0.6 \sim 2/3$, supporting the behavior $\alpha \sim 1/W$ [cf. (8) and Sec. V]. For the KHA ($W = 4$), a similar fit gives $\alpha \approx 0.17$, (only ES levels with $S_A \leq 3$ were fitted). Results of the fit are shown in Fig. 4 as squares and are in excellent agreement with the DMRG data. Also, the agreement is better at larger system sizes (compare in Fig. 4 DMRG data for the THA at $W = 9$ and 6), confirming that (8) holds in the asymptotic regime $V \rightarrow \infty$.

V. FINITE-SIZE AND BOUNDARY EFFECTS IN TOS STRUCTURES

One crucial consequence of the correspondence between TOS and entanglement spectra, according to (8), is that the spacing within low-lying ES multiplets is $\sim 1/\sqrt{V} \approx 1/W$. Oppositely, the entanglement gap between the TOS part and the rest of the spectrum remains finite in the thermodynamic limit (or vanishes logarithmically, cf. the discussion in Sec. IV A). These features are numerically demonstrated in Sec. V A.

The effect of boundary conditions on TOS structures is instead discussed in Sec. V B, by examining the ES of the J_1 - J_2 KHA on the torus. The most notable consequence of the torus geometry is that the number of boundaries between the two subsystems is doubled. However, although this gives rise to quantitative differences compared to the cylinder geometry,

qualitative features [i.e., TOS behavior as $S_A(S_A + 1)$ and TOS multiplets counting] remain unchanged, signaling the bulk origin of the TOS structures.

A. Entanglement gap and TOS level spacing: finite-size scaling analysis

The structure of the lower part of the ES (TOS structure) can be characterized using the entanglement gap Δ_0 and the tower of states level spacing δ .¹⁵ These are defined pictorially in Fig. 5(a). More formally, δ is the “distance” between the two lowest levels in the sectors with $S_A = 0, 1$ (respectively $S_A = 1/2, 3/2$ for S_A half integer), i.e., $\delta \equiv \xi_1 - \xi_0$ with ξ_σ the lowest ES level in the sector with $S_A = \sigma$. This is also a measure of the “slope” of the TOS structure. The entanglement gap Δ_0 measures, instead, the separation between the TOS structure and the higher ES levels. Since it depends weakly on S_A (cf. Figs. 2 and 3), here we consider the gap Δ_0 in the lowest spin sector [$S_A = 0(1/2)$ for integer (half-integer) S_A].

Figure 5(b) plots Δ_0 as a function of the boundary length $2 \leq W \leq 9$ for both the kagome and triangular J_1 - J_2 Heisenberg models ($J_2/J_1 = -1$). The ES is for half of the system and data are DMRG for cylinders with fixed aspect ratio $W/L = 1/2$. For both models, the extrapolation to infinite cylinders (assuming the behavior $1/\sqrt{V} \sim 1/W$) (dotted lines) suggests a finite value (crosses in the figure) of Δ_0 (see, however, the discussion in Sec. IV A).

Figure 5(c) shows δ versus $1/W$. In order to avoid parity effects (in V), we plot δ/dS_A^2 , with $dS_A^2 \equiv S_A(S_A + 1)|_1 - S_A(S_A + 1)|_0$. Clearly, this is vanishing for infinite cylinders ($W \rightarrow \infty$). The expected behavior $\delta \sim 1/\sqrt{V} \sim 1/W$ [cf. (8)] is fully confirmed for the J_1 - J_2 THA (rhombi in the figure,

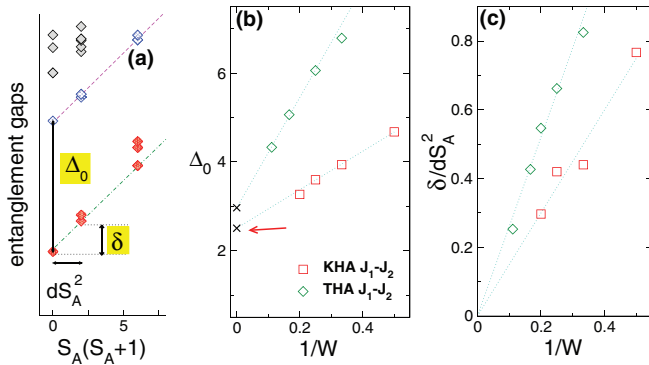


FIG. 5. (Color online) Finite-size scaling of the entanglement gap Δ_0 and the tower of states spacing δ in the J_1 - J_2 Heisenberg model on the kagome (KHA) and triangular (THA) lattice (at $J_2/J_1 = -1$). DMRG data for the ES of half the system (cylindrical geometry as in Fig. 1 with fixed aspect ratio $W/L = 1/2$). (a) Pictorial definitions of entanglement gap and tower level spacing: δ is the “distance” between the two lowest levels in the ES (here respectively in the sectors $S_A = 0$ and $S_A = 1$). Δ_0 is the gap between the TOS structure and higher ES levels in the $S_A = 0$ sector. (b) Δ_0 as a function of $1/W$: the gap is finite in the limit $W \rightarrow \infty$. Dotted lines are fits to $A + B/W$. The extrapolated values for A are shown as crosses. (c) Vanishing of the tower level spacing δ in the thermodynamic limit. To avoid odd-even effects, δ is divided by $dS_A^2 = 2, 3$ for, respectively, integer and half-integer S_A . δ/dS_A^2 plotted vs $1/W$. Dotted lines are fits to A/W .

dotted line is a fit to A/W), while for the J_1 - J_2 KHA the scenario is less robust due to residual parity effects.

B. Periodic boundary conditions: ES of the KHA on the torus

Boundary conditions, in particular, number of boundaries between the two subsystems, can affect dramatically the ES (and the entanglement entropies). For instance, in gapped (nontopological) one-dimensional and two-dimensional systems the ES is a boundary local quantity^{4,15} and a change in the number of boundaries leads to quantitative and qualitative changes in the ES. It is interesting to clarify the effect of boundary conditions on the TOS structures outlined in Sec. IV. To this purpose here we consider the ES of the J_1 - J_2 KHA on the torus.

This is illustrated in Fig. 6 (ES for half-torus, DMRG data at $J_2/J_1 = -1$). Data points are for both $W = 3$ and 4 [at fixed aspect ratio $W/L = 1/2$, respectively, (a) and (b) in Fig. 6]. The main features of low-lying ES multiplets are the same as in the cylindrical geometry (compare Fig. 6 with Fig. 2). The linear behavior of the ES as function of $S_A(S_A + 1)$ (Pisa tower structure) is clearly visible and an apparent gap divides the low-lying ES multiplets from the rest. The number of levels

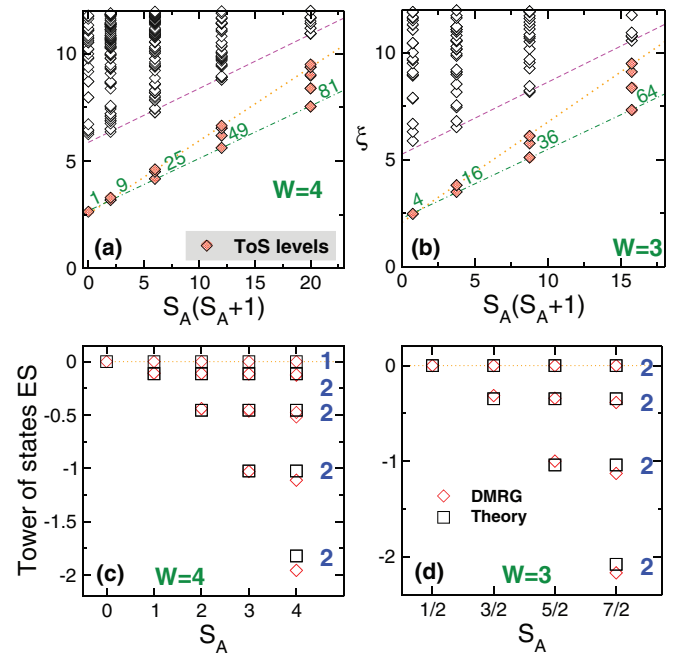


FIG. 6. (Color online) ES of the kagome J_1 - J_2 Heisenberg model (KHA) on the torus. Data is DMRG at $J_2/J_1 = -1$ and $W = L/2 = 3$, $W = L/2 = 4$ [respectively, panels (a) and (b) in the figure]. The ES is for half of the torus: ES levels ξ plotted vs the subsystem spins $S_A(S_A + 1)$. Filled rhombi denote the tower of states (TOS) ES levels. The numbers are the total numbers of TOS levels in each sector S_A . The dashed-dotted line highlights the linear behavior [with respect to $S_A(S_A + 1)$ of TOS levels]. The dashed line marks the higher part of the ES. (c) and (d) Enlarged view of TOS structures: TOS ES levels [same data as in (a) and (b)] shifted by the value of the highest level [dotted line in (a) and (b)] plotted vs S_A . The squares denote the (one parameter) fit to the expected result in the large volume limit [cf. formula (8)]. The number of degenerate SU(2) multiplets is shown in blue.

building the TOS sector with fixed S_A is given as $(2S_A + 1)^2$ (i.e., as for kagome cylinders).

The effective entanglement Hamiltonian \mathcal{H}_E describing the TOS structure is given by (8). This is demonstrated in Figs. 6(c) and 6(d). ES levels (only TOS levels are shown) are plotted versus the block spin S_A . Each ES tower (at fixed S_A) was shifted by subtracting the contribution of the largest level (in that sector). Squares are one parameter fits to $\alpha[(S_A^z)^2 + s_0]$ (α is the fitting parameter, cf. Sec. IV C), which give $\alpha \approx 0.16$ and $\alpha \approx 0.11$ for, respectively, $W = 3$ and 4. It is instructive to observe that for kagome cylinders one obtains $\alpha \approx 0.17$ at $W = 4$ (cf. Sec. IV C). The reduction of α (by a factor ≈ 2) has to be attributed to the two boundaries (between the subsystems).

VI. CONCLUSIONS AND OUTLOOK

In this paper, we studied the *ground-state* entanglement spectrum in SU(2)-broken phases. We considered the two-dimensional J_1 - J_2 Heisenberg model on both the triangular and kagome lattice, restricting ourselves to antiferromagnetic(ferromagnetic) $J_1(J_2)$ and $J_2/J_1 = -1$.

On both lattices the ground state of the model displays magnetic order [and SU(2) symmetry breaking, in the thermodynamic limit]. This is associated with the appearance in the finite-size (spin-resolved) energy spectrum of a special type of low-lying excitations, forming the so-called tower of states (TOS). The TOS structure is divided from the higher part of the spectrum (at least for large system sizes) by an energy gap. The number of TOS energy levels in each spin sector S reflects the selected symmetry breaking pattern and is given as $(2S + 1)^2$.

In this work, we demonstrated that this structure is reflected in the lower part of the *ground-state* ES. Precisely, the ES exhibits families of low-lying levels, which are divided from the rest by an *entanglement gap*, and form a TOS-like structure. The number of TOS levels in a given (subsystem) spin sector S_A is $(2S_A + 1)^2$, clearly reflecting the corresponding counting in the energy TOS. Moreover, finite-size behaviors of low-lying ES levels can be understood in terms of the energy TOS. All these features can be expressed quantitatively as a mapping between the low-lying structure (excitations) of the physical Hamiltonian \mathcal{H} and of the entanglement Hamiltonian \mathcal{H}_E [expressed by formula (8)].

On the methodological side, our results suggest that entanglement (tower of states) spectroscopy, combined with SU(2)-symmetric DMRG, could be used as a tool for characterizing SU(2)-broken phases. Finally, we would like to mention that an intriguing research direction originating from this work would be to investigate how the TOS structure evolves in the J_1 - J_2 kagome Heisenberg model as the $J_2 = 0$ point is approached. In particular, it would be interesting to characterize how the low-lying ES levels rearrange to reflect the onset of the Z_2 spin liquid found in Refs. 54 and 55.

ACKNOWLEDGMENTS

V.A. thanks Andreas Läuchli for very useful discussions and collaboration in a related project. V.A. and S.D. thank the MIPPKS of Dresden, where this work was partly done, for the hospitality during the workshop “Entanglement Spectra in Complex Quantum Wave functions.” U.S. and S.D. acknowledge funding by DFG through NIM and SFB/TR 12.

¹L. Amico, R. Fazio, A. Osterloh, and V. Vedral, *Rev. Mod. Phys.* **80**, 517 (2008); J. Eisert, M. Cramer, and M. B. Plenio, *ibid.* **82**, 277 (2010).

²H. Li and F. D. M. Haldane, *Phys. Rev. Lett.* **101**, 010504 (2008).

³I. Peschel and V. Eisler, *J. Phys. A: Math. Theor.* **42**, 504003 (2009).

⁴V. Alba, M. Haque, and A. M. Läuchli, *Phys. Rev. Lett.* **108**, 227201 (2012).

⁵L. Lepori, G. De Chiara, and A. Sanpera, *Phys. Rev. B* **87**, 235107 (2013).

⁶P. Calabrese and A. Lefevre, *Phys. Rev. A* **78**, 032329 (2008).

⁷G. De Chiara, L. Lepori, M. Lewenstein, and A. Sanpera, *Phys. Rev. Lett.* **109**, 237208 (2012).

⁸A. M. Läuchli, *arXiv:1303.0741*.

⁹N. Regnault, B. A. Bernevig, and F. D. M. Haldane, *Phys. Rev. Lett.* **103**, 016801 (2009); N. Bray-Ali, L. Ding, and S. Haas, *Phys. Rev. B* **80**, 180504(R) (2009); L. Fidkowski, *Phys. Rev. Lett.* **104**, 130502 (2010); A. M. Läuchli, E. J. Bergholtz, J. Suorsa, and M. Haque, *ibid.* **104**, 156404 (2010); R. Thomale, A. Sterdyniak, N. Regnault, and B. A. Bernevig, *ibid.* **104**, 180502 (2010); H. Yao and X. L. Qi, *ibid.* **105**, 080501 (2010); E. Prodan, T. L. Hughes, and B. A. Bernevig, *ibid.* **105**, 115501 (2010); F. Pollmann, A. M. Turner, E. Berg, and M. Oshikawa, *Phys. Rev. B* **81**, 064439 (2010); M. Kargarian and G. A. Fiete, *ibid.* **82**, 085106 (2010);

A. M. Turner, Y. Zhang, and A. Vishwanath, *ibid.* **82**, 241102(R) (2010); Z. Papic, B. A. Bernevig, and N. Regnault, *Phys. Rev. Lett.* **106**, 056801 (2011); L. Fidkowski, T. S. Jackson, and I. Klich, *ibid.* **107**, 036601 (2011); J. Dubail and N. Read, *ibid.* **107**, 157001 (2011); J. Schliemann, *Phys. Rev. B* **83**, 115322 (2011); T. L. Hughes, E. Prodan, and B. A. Bernevig, *ibid.* **83**, 245132 (2011); N. Regnault and B. A. Bernevig, *Phys. Rev. X* **1**, 021014 (2011); X. L. Qi, H. Katsura, and A. W. W. Ludwig, *Phys. Rev. Lett.* **108**, 196402 (2012); D. Poilblanc, N. Schuch, D. Perez-Garcia, and J. I. Cirac, *Phys. Rev. B* **86**, 014404 (2012); B. Swingle and T. Senthil, *ibid.* **86**, 045117 (2012); N. Schuch, D. Poilblanc, J. I. Cirac, and D. Perez-Garcia, *Phys. Rev. Lett.* **111**, 090501 (2013); D. Poilblanc and N. Schuch, *Phys. Rev. B* **87**, 140407 (2013); J. Schliemann, *New J. Phys.* **15**, 053017 (2013); Z. Liu, D. L. Kovrizhin, and E. J. Bergholtz, *Phys. Rev. B* **88**, 081106(R) (2013).

¹⁰J. I. Cirac, D. Poilblanc, N. Schuch, and F. Verstraete, *Phys. Rev. B* **83**, 245134 (2011).

¹¹S. Tanaka, R. Tamura, and H. Katsura, *Phys. Rev. A* **86**, 032326 (2012).

¹²J. Lou, S. Tanaka, H. Katsura, and N. Kawashima, *Phys. Rev. B* **84**, 245128 (2011).

¹³A. J. A. James and R. M. Konik, *Phys. Rev. B* **87**, 241103(R) (2013).

¹⁴M. A. Metlitski and T. Grover, *arXiv:1112.5166*.

- ¹⁵V. Alba, M. Haque, and A. M. Läuchli, *Phys. Rev. Lett.* **110**, 260403 (2013).
- ¹⁶B. Bernu, C. Lhuillier, and L. Pierre, *Phys. Rev. Lett.* **69**, 2590 (1992).
- ¹⁷B. Bernu, P. Lecheminant, C. Lhuillier, and L. Pierre, *Phys. Rev. B* **50**, 10048 (1994); I. Rousochatzakis, A. M. Läuchli, and F. Mila, *ibid.* **77**, 094420 (2008); I. Rousochatzakis, A. M. Läuchli, and R. Moessner, *ibid.* **85**, 104415 (2012).
- ¹⁸P. Lecheminant, B. Bernu, C. Lhuillier, and L. Pierre, *Phys. Rev. B* **52**, 6647 (1995).
- ¹⁹P. Lecheminant, B. Bernu, C. Lhuillier, L. Pierre, and P. Sindzingre, *Phys. Rev. B* **56**, 2521 (1997).
- ²⁰A. M. Läuchli, J. C. Domenge, C. Lhuillier, P. Sindzingre, and M. Troyer, *Phys. Rev. Lett.* **95**, 137206 (2005).
- ²¹N. Shannon, T. Momoi, and P. Sindzingre, *Phys. Rev. Lett.* **96**, 027213 (2006).
- ²²P. Sindzingre and C. Lhuillier, *Europhys. Lett.* **88**, 27009 (2009).
- ²³K. Penc and A. M. Läuchli, *Springer Ser. Solid-State Sci.* **164**, 331 (2011).
- ²⁴C. Lhuillier, [arXiv:cond-mat/0502464v1](https://arxiv.org/abs/cond-mat/0502464v1).
- ²⁵T. Oguchi, *J. Phys. Soc. Jpn. Suppl.* **52**, 183 (1983).
- ²⁶T. Jolicoeur and J. C. Le Guillou, *Phys. Rev. B* **40**, 2727 (1989).
- ²⁷S. J. Miyake, *J. Phys. Soc. Jpn.* **61**, 983 (1992).
- ²⁸R. R. P. Singh and D. A. Huse, *Phys. Rev. Lett.* **68**, 1766 (1992).
- ²⁹A. V. Chubukov, S. Sachdev, and T. Senthil, *J. Phys.: Condens. Matter* **6**, 8891 (1994).
- ³⁰A. L. Chernyshev and M. E. Zhitomirsky, *Phys. Rev. B* **79**, 144416 (2009).
- ³¹L. Capriotti, A. E. Trumper, and S. Sorella, *Phys. Rev. Lett.* **82**, 3899 (1999).
- ³²W. H. Zheng, J. O. Fjærestad, R. R. P. Singh, R. H. McKenzie, and R. Coldea, *Phys. Rev. B* **74**, 224420 (2006).
- ³³S. R. White and A. L. Chernyshev, *Phys. Rev. Lett.* **99**, 127004 (2007).
- ³⁴J. B. Marston and C. Zeng, *J. Appl. Phys.* **69**, 5962 (1991).
- ³⁵C. Zeng and V. Elser, *Phys. Rev. B* **42**, 8436 (1990).
- ³⁶M. B. Hastings, *Phys. Rev. B* **63**, 014413 (2000).
- ³⁷P. Nikolic and T. Senthil, *Phys. Rev. B* **68**, 214415 (2003).
- ³⁸R. R. P. Singh and D. A. Huse, *Phys. Rev. B* **76**, 180407(R) (2007).
- ³⁹R. R. P. Singh and D. A. Huse, *Phys. Rev. B* **77**, 144415 (2008).
- ⁴⁰Y. Iqbal, F. Becca, and D. Poilblanc, *New J. Phys.* **14**, 115031 (2012).
- ⁴¹L. Messio, B. Bernu, and C. Lhuillier, *Phys. Rev. Lett.* **108**, 207204 (2012).
- ⁴²K. Yang, L. K. Warman, and S. M. Girvin, *Phys. Rev. Lett.* **70**, 2641 (1993).
- ⁴³M. Hermele, Y. Ran, P. A. Lee, and X. G. Wen, *Phys. Rev. B* **77**, 224413 (2008).
- ⁴⁴Y. Iqbal, F. Becca, and D. Poilblanc, *Phys. Rev. B* **84**, 020407 (2011).
- ⁴⁵Y. Ran, M. Hermele, P. A. Lee, and X. G. Wen, *Phys. Rev. Lett.* **98**, 117205 (2007).
- ⁴⁶S. Ryu, O. I. Motrunich, J. Alicea, and M. P. A. Fisher, *Phys. Rev. B* **75**, 184406 (2007).
- ⁴⁷S. Sachdev, *Phys. Rev. B* **45**, 12377 (1992).
- ⁴⁸F. Wang and A. Vishwanath, *Phys. Rev. B* **74**, 174423 (2006).
- ⁴⁹Y. M. Lu, Y. Ran, and P. A. Lee, *Phys. Rev. B* **83**, 224413 (2011).
- ⁵⁰G. Misguich, D. Serban, and V. Pasquier, *Phys. Rev. Lett.* **89**, 137202 (2002).
- ⁵¹H. C. Jiang, Z. Y. Weng, and D. N. Sheng, *Phys. Rev. Lett.* **101**, 117203 (2008).
- ⁵²Y. Huh, M. Punk, and S. Sachdev, *Phys. Rev. B* **84**, 094419 (2011).
- ⁵³V. Kalmeyer and R. B. Laughlin, *Phys. Rev. B* **39**, 11879 (1989).
- ⁵⁴S. Yan, D. Huse, and S. White, *Science* **332**, 1173 (2011).
- ⁵⁵S. Depenbrock, I. P. McCulloch, and U. Schollwöck, *Phys. Rev. Lett.* **109**, 067201 (2012).
- ⁵⁶H. C. Jiang, Z. Wang, and L. Balents, *Nat. Phys.* **8**, 902 (2012).
- ⁵⁷S. R. White, *Phys. Rev. Lett.* **69**, 2863 (1992).
- ⁵⁸U. Schollwöck, *Rev. Mod. Phys.* **77**, 259 (2005).
- ⁵⁹U. Schollwöck, *Ann. Phys.* **326**, 96 (2011).
- ⁶⁰S. R. White, *Phys. Rev. Lett.* **77**, 3633 (1996).
- ⁶¹S. R. White and D. J. Scalapino, *Phys. Rev. Lett.* **80**, 1272 (1998).
- ⁶²S. R. White and D. J. Scalapino, *Phys. Rev. Lett.* **81**, 3227 (1998).
- ⁶³E. M. Stoudenmire and S. R. White, *Ann. Rev. Cond. Mat. Phys.* **3**, 111 (2012).
- ⁶⁴P. W. Anderson, *Phys. Rev.* **86**, 694 (1952).
- ⁶⁵M. Gross, E. Sanchez-Velasco, and E. D. Siggia, *Phys. Rev. B* **40**, 11328 (1989).
- ⁶⁶D. S. Fisher, *Phys. Rev. B* **39**, 11783 (1989).
- ⁶⁷P. Azaria, B. Delamotte, and D. Mouhanna, *Phys. Rev. Lett.* **70**, 2483 (1993).
- ⁶⁸M. A. Metlitski and T. Grover (private communication).
- ⁶⁹A. B. Kallin, I. González, M. B. Hastings, and R. G. Melko, *Phys. Rev. Lett.* **103**, 117203 (2009).
- ⁷⁰M. B. Hastings, I. González, A. B. Kallin, and R. G. Melko, *Phys. Rev. Lett.* **104**, 157201 (2010).
- ⁷¹H. F. Song, N. Laflorencie, S. Rachel, and K. Le Hur, *Phys. Rev. B* **83**, 224410 (2011).